redin Revista Facultad de Ingeniería, Universidad de Antioquia, No. 83, pp. 20-30, 2017

# Study of the visible light activity of Pt and Au-$TiO_2$ photocatalysts in organic pollutants degradation

## Estudio de la actividad de los fotocatalizadores Pt and Au-$TiO_2$ en la degradación de contaminantes orgánicos bajo luz visible

**Jairo Antonio Cubillos-Lobo[1*], Julie Joseane Murcia-Mesa[1], Jhonatan Ricardo Guarín-Romero[1], Hugo Alfonso Rojas-Sarmiento[1], María del Carmen Hidalgo-López[2], José Antonio Navío-Santos[2]**

[1] Grupo de Catálisis, Escuela de Ciencias Químicas, Universidad Pedagógica y Tecnológica de Colombia. Avenida Central del Norte 39-115. C. P. 150007. Tunja, Colombia.
[2]Instituto de Ciencia de Materiales de Sevilla (ICMS), Consejo Superior de Investigaciones Científicas CSIC - Universidad de Sevilla. Calle Américo Vespucio 49. C. P. 41092. Sevilla, España.

**ARTICLE INFO**
Received January 24, 2017
Accepted April 17, 2017

**KEYWORDS**
Pt-S-$TiO_2$, Au-S-$TiO_2$, UV-Visible, visible light, pollutants photodegradation

Pt-S-$TiO_2$, Au-S-$TiO_2$, UV-Visible, luz visible, degradación de contaminantes

**ABSTRACT:** Pt-$TiO_2$ and Au-$TiO_2$ photocatalysts were prepared by noble metal photodeposition on sulfated $TiO_2$. It was observed that optical absorption, oxidation state and particle size of the metallic species (Pt or Au) play an important role in the $TiO_2$ photocatalytic activity under visible-light irradiation. Photocatalytic activity of the bare $TiO_2$ powder in the phenol and methyl orange degradation increased with the sulfation and metal addition. The highest degradation rate under UV-Visible and visible light irradiation was obtained on Pt-S-$TiO_2$ photocatalyst; this is mainly due to the optical properties of $TiO_2$ induced by platinization and also to the good distribution and low Pt particles size. It was also found that this catalyst has a good stability after two cycles of reaction in the phenol photodegradation under UV-Visible light irradiation. The Pt-S-$TiO_2$ photocatalyst was also active under solar light and under the environmental conditions of the city of Tunja (Boyacá), Colombia.

**RESUMEN:** Los fotocatalizadores Pt-$TiO_2$ y Au-$TiO_2$ se prepararon por fotodeposición del metal noble sobre el $TiO_2$ sulfatado. Se encontró que las propiedades ópticas, el estado de oxidación y el tamaño de partícula de las especies metálicas (Pt o Au) juegan un papel fundamental en la actividad fotocatalítica del $TiO_2$ bajo luz visible. La actividad fotocatalítica del $TiO_2$ en la degradación de fenol y naranja de metilo aumentó significativamente a través de los tratamientos de sulfatación y metalización de este óxido. La más alta velocidad de degradación bajo luz UV-Visible y visible, se alcanzó usando el fotocatalizador Pt-S-$TiO_2$; esto se debe principalmente a la modificación de las propiedades ópticas del $TiO_2$ inducidas por la platinización, también a la buena distribución y al pequeño tamaño de las partículas de Pt. Se encontró, además, que este catalizador presenta una buena estabilidad después de dos ciclos de reacción en la degradación de fenol bajo luz UV-Visible. El fotocatalizador Pt-S-$TiO_2$ fue activo también bajo luz solar directa y bajo las condiciones medioambientales de la ciudad de Tunja (Boyacá), Colombia.

## 1. Introduction

Photocatalysis is an effective and promising process for the destruction of contaminants such as microorganisms, phenolic compounds and dyes in water sources, by using solar or artificial light irradiation. Titanium dioxide has been extensively studied and used as photocatalyst in different chemical reactions [1-3]; however, the high recombination rate of the electron-hole pairs reduces the $TiO_2$ photoactivity. The application of this oxide as a photocatalyst for visible light-induced chemical reactions has been limited, mainly due to its large band-gap energy (3.2 eV for anatase $TiO_2$), which requires ultraviolet (UV) light to be activated [3].

In order to improve $TiO_2$ photoefficiency under UV-Visible and visible light, different strategies have been developed; thus, it has been reported that sulfation of $TiO_2$ surface results in the generation of superficial oxygen vacancies thus leading to the enhancement of the UV-photocatalytic activity of the $TiO_2$ through the improvement of both charge

* Corresponding author: Jairo Antonio Cubillos Lobo
e-mail: jairo.cubillos@uptc.edu.co
ISSN 0120-6230
e-ISSN 2422-2844
DOI: 10.17533/udea.redin.n83a03

separation and carriers lifetime. Alternatively, deposition of noble metal particles on surface and/or doping with nonmetals may be done to tailor the electronic and optical properties of $TiO_2$ [4-7].

The noble metal nanoparticles deposited on $TiO_2$ surface act as collectors of electrons photogenerated, thus reducing the recombination rate [8-11]. Though less studied, it has also been reported that doping $TiO_2$ with noble transition metals leads to photocatalysts active under visible light [12, 13].

The beneficial or detrimental effect of the noble metal deposition on the $TiO_2$ photoactivity has been extensively discussed in the literature [1-10,13-15] and it has been observed that under the experimental conditions used in this work, the sulfation pretreatment and the noble metal addition are important factors influencing positively the $TiO_2$ activity in the water pollutants photodegradation under visible irradiation.

The main objective of this study was to evaluate the photocatalytic activity of $TiO_2$ modified by sulfation and Pt or Au deposition under visible irradiation. For comparison, activity under UV-Visible light was also evaluated. The activity of the materials prepared was evaluated in the phenol and methyl orange photodegradation reactions.

# 2. Experimental

## 2.1. Photocatalysts synthesis procedure

Commercial $TiO_2$ Aeroxide Evonik P25, used as a reference material was employed as received. The experimental conditions used in the synthesis of the catalysts were previously described by J.J Murcia *et al.* [9] and M. Maicu *et al.* [10].

In a typical procedure, $TiO_2$ used as starting material was prepared by the hydrolysis of titanium tetraisopropoxide (Aldrich, 97%) in isopropanol solution (1.6 M) by the slow addition of distilled water (volume ratio isopropanol/water 1:1). Afterward, the generated precipitate was filtered, dried at 110°C overnight and calcined at 650 °C for 2h. The sample thus obtained was called bare $TiO_2$.

Sulfation treatment was applied to $TiO_2$ before calcination; the powders were sulfated by immersion in $H_2SO_4$ aqueous solution 1 M for 1 h and afterward calcinated at 650 ºC for 2 h (S-$TiO_2$). Sulfation treatment was carried out for two reasons; on one hand, previous results have shown that sulfation stabilizes the anatase phase up to high temperatures and protect the catalyst from the loss of surface area by sintering [10]. On the other hand, at the calcination temperature of 650 ºC, the elimination of sulfate groups promotes the creation of high number of oxygen vacancies, which have been reported as preferential sites for noble metal adsorption [16].

The S-$TiO_2$ powder was modified by noble metal addition, using the photochemical deposition method. Hexachloroplatinic acid ($H_2PtCl_6$, Aldrich 99.9%) or Gold (III) chloride trihydrate ($HAuCl_4.3H_2O$, Aldrich 99.9%) were used as metal precursors for Pt and Au, respectively. Under an inert atmosphere ($N_2$), a suspension of S-$TiO_2$ in distilled water containing isopropanol (Merck 99.8%) which acts as sacrificial donor was prepared. Then, the metal precursor was added. The nominal Pt or Au loading was 0.5% weight total to $TiO_2$; the final pH of this suspension was 3. Finally, the photochemical deposition of Pt or Au was performed by illuminating the suspensions with an Osram Ultra-Vitalux lamp (300W); this lamp has a sun-like radiation spectrum and a main emission line in the UVA range at 365 nm. The light intensities on the $TiO_2$ surface were 60 and 0.15 W/m$^2$ for Pt and Au photochemical deposition, respectively. Those light intensities were chosen according to previous results focused on the synthesis of photocatalysts with the best properties for the two different metals [9, 10]. The illumination time at those intensities was fixed at 120 min.

After photodeposition, the powders were recovered by filtration and dried at 110 °C overnight. The metallized samples were called Pt-S-$TiO_2$ and Au-S-$TiO_2$.

## 2.2. Characterization of the photocatalysts

BET surface areas ($S_{BET}$) of all samples were evaluated by $N_2$ adsorption measurement with a Micromeritics ASAP 2010 instrument. Degasification of the samples was performed at 150 ºC for 30 min in He flow.

Crystalline phase composition and degree of crystallinity of the samples were estimated by X-ray diffraction (XRD). XRD patterns were obtained on a Siemens D-501 diffractometer with Ni filter and graphite monochromator using Cu K$\alpha$ radiation. Crystallite sizes were calculated from the line broadening of the main anatase X-ray diffraction peak (1 0 1) by using the Scherrer equation. Peaks were fitted by using a Voigt function.

Light absorption properties of the samples were studied by UV–Vis spectroscopy. The Diffuse Reflectance UV–Vis Spectra (UV–Vis DRS) were recorded on a Varian spectrometer model Cary 100 equipped with an integrating sphere and using $BaSO_4$ as reference. Band-gaps values were calculated from the corresponding Kubelka–Munk functions, F(R∞), which are proportional to the absorption of radiation, by plotting $(F(R\infty) \times h\upsilon)^{1/2}$ against $h\upsilon$.

Chemical composition and total platinum and gold content in the samples were determined by X-ray fluorescence spectrometry (XRF) in a Panalytical Axios sequential spectrophotometer equipped with a rhodium tube as the source of radiation. XRF measurements were performed onto pressed pellets (sample included in 10 wt.% of wax). Transmission electron microscopy (TEM) was performed in a Philips CM 200 microscope. The samples were dispersed in ethanol using an ultrasonicator and dropped on a carbon grid.

X-ray photoelectron spectroscopy (XPS) studies were carried out on a Leybold-Heraeus LHS-10 spectrometer, working with constant pass energy of 50 eV. The spectrometer main chamber, working at a pressure <$2\times10^{-9}$ Torr, is equipped with an EA-200 MCD hemispherical electron analyzer with a dual X-ray source working with Al Kα (hυ = 1486.6 eV) at 120 W and 30 mA. C 1s signal (284.6 eV) was used as internal energy reference in all the experiments. Samples were outgassed in the pre-chamber of the instrument at 150 °C up to a pressure <$2\times10^{-8}$ Torr to remove chemisorbed water.

## 2.3. Water pollutants photodegradation

The photocatalytic activity of the samples prepared was tested in the degradation of water pollutants. Phenol and methyl orange (MO) were selected as model molecules. Photocatalytic tests were carried out using a discontinuous batch system, this includes a 400 mL pyrex reactor enveloped by an aluminum foil, filled with an aqueous suspension (250 mL) containing 50 ppm of phenol (0.53 mM) or MO (0.15 mM) and the photocatalyst (1 g/L). This system was illuminated through a UV-transparent Plexiglas® top window (threshold absorption at 250 nm) by an Osram Ultra-Vitalux lamp (300 W) with sun-like radiation spectrum and a main line in the UVA range at 365 nm.

The photocatalytic reactions were carried out using two different irradiation conditions UV-Visible and visible light irradiation. The intensity of the incident UV-Visible light on the solution was measured with a PMA 2200 UVA photometer (Solar Light Co.) being ca 120 W/m$^2$ (UVA PMA2110 sensor; spectral response 320–400 nm). The visible photocatalytic experiments were performed by using a polyester UV filter sheet (Edmund Optics) showing 99.9% of absorbance below 400 nm (0.15 W/m$^2$ for $\lambda < 400$ nm and 150 W/m$^2$ for $\lambda > 400$ nm).

In order to favor the adsorption–desorption equilibrium, prior to irradiation the suspension was magnetically stirred for 10 min in dark. Magnetic stirring and a constant oxygen flow of 35 L/h as an oxidant were used to produce a homogeneous suspension of the photocatalyst in the solution. All photocatalytic tests started at pH ca. 6 and the total reaction time was 120 min.

During the phenol photoreaction, samples were collected at different times and measured by HPLC, using an Agilent Technologies 1200 chromatograph, which was equipped with UV–Vis detector and an Elipse XDB-C18 column (5$\mu$m, 4.6 mm ×150 mm). The HPLC analysis was carried out using water/methanol (65:35) as mobile phase, a flow rate of 0.8 mL/min and 40 °C.

In order to evaluate the dye discoloration rate, the concentration of methyl orange during the photodegradation reaction was analyzed by UV–Visible spectroscopy, considering the main peak of this dye located at 465 nm [17]. For this analysis a GBC 911 instrument was used.

From HPLC and UV-Vis spectrophotometry, it was possible to determine the substrate concentration and the initial degradation rate. This rate was calculated considering the first 60 minutes of reaction, and by using the Eq. (1).

$$V = \frac{(K)(C_0)}{(t)} \quad (1)$$

Where:

$K$= Reaction constant, obtained from the slope of the degradation profile graph (substrate concentration *Vs* reaction time)

$C_0$ = Starting concentration of the substrate [mg.L$^{-1}$]

$t$ = Time (s)

Photolysis tests of phenol and MO under UV-Visible and visible light irradiations and in absence of catalyst were carried out. Under the experimental conditions used in this work, substrate photolysis was not observed in any case. Reproducibility of the measurements was ensured by double testing of selected samples.

Series of tests under direct solar light were also carried out, for these experiments, the same setup employed in the artificial light tests, were used. In this case, the batch reactor was exposed directly to solar light, thus the phenol and MO photodegradation reactions were carried out under the environmental condition of the city of Tunja (Boyacá), Colombia (5°32′7″North latitude 73°22′04″E).

# 3. Results and discussion

## 3.1. Characterization of the photocatalysts

As it was mentioned in the experimental section and in order to correlate the physico-chemical properties of the catalysts with their photocatalytic activity, all the materials were widely characterized by using different techniques and the results obtained are presented below.

### $N_2$ physisorption

The specific surface areas ($S_{BET}$) of the $TiO_2$ powders after calcination at 650°C are listed in Table 1. As it can be observed, the BET surface area of bare $TiO_2$ is 11 m$^2$/g. For the sample with the sulfation pretreatment, this value considerably increases. The lower $S_{BET}$ in the bare oxide can be ascribed to the larger degree of particles sintering during the calcination process. As it has been reported previously by some of us, the sulfation pretreatment has a protective effect of the $TiO_2$ surface area avoiding the sintering during the calcination process [10]. For the platinized sample, a slight decrease of the $S_{BET}$ value with the metal deposition was detected, probably due to pore blocking by metal nanoparticles homogeneously distributed on surface.

**Table 1 Characterization results of bare and modified $TiO_2$.**

| Photocatalysts | $S_{BET}$ ($m^2/g$) | $D_{Anatase}$ (nm) | Band gap (eV) | Binding energy (eV) | | O/Ti |
|---|---|---|---|---|---|---|
| | | | | Ti $2p_{3/2}$ | O 1s | |
| Bare $TiO_2$ | 11 | 17 | 3.30 | 458.5 | 529.8 | 1.96 |
| S-$TiO_2$ | 58 | 20 | 3.20 | 458.5 | 529.8 | 1.70 |
| Pt-S-$TiO_2$ | 49 | 20 | 3.17 | 458.4 | 529.6 | 1.91 |
| Au-S-$TiO_2$ | 60 | 19 | 3.20 | 458.5 | 529.8 | 1.88 |

## X-ray diffraction (XRD)

Crystalline phase composition and crystallinity degree of the samples were studied by XRD and the patterns are presented in Figure 1. For the bare $TiO_2$ sample peaks of anatase (major peaks: 25.3°, 38.0°, 48.0° and 54.7° 2θ) and rutile (main peak located at 27.4° 2θ) phases were observed. In the sulfated and metallized samples, only anatase peaks were detected. The stabilization of anatase phase of the $TiO_2$ by the sulfation pretreatment can be noticed here as no traces of rutile were found even after the high calcination temperature used during the preparation of the catalysts.

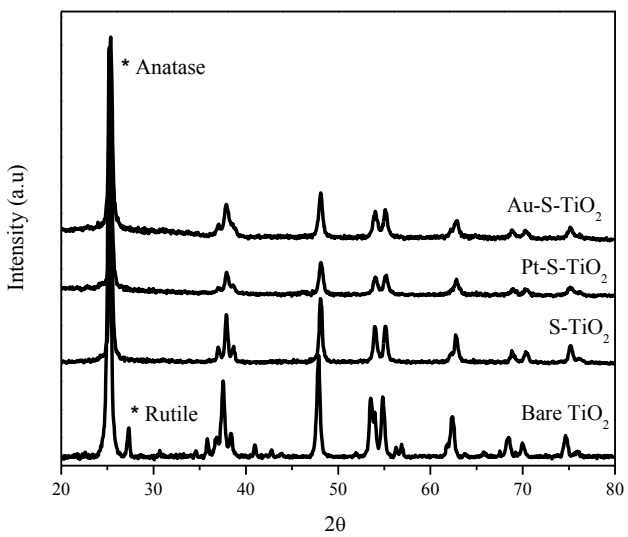


**Figure 1 XRD patterns for bare and metallized $TiO_2$**

The anatase crystallite size in the different samples was determined from the broadening of corresponding X-ray diffraction peaks by using Scherrer equation and these data are listed in Table 1. As it can be observed, for sulfated samples the anatase crystallite size was about 20 nm and the bare $TiO_2$ sample presented a lower value of 17 nm.

No peaks ascribed to platinum or gold species were detected in the XRD patterns of the metallized samples; surely due to the low metal content in the samples or due to the detection limit of this technique.

## UV-Vis DR Spectra

Figure 2 displays the UV–Vis DR spectra for all the analyzed photocatalysts in a wavelength range between 200 and 800 nm. The characteristic sharp absorption threshold of $TiO_2$ around 350 nm can be observed for all the samples. As it is clearly shown in Figure 2, the samples exhibit different colors depending on the composition of each material. Thus bare and S-$TiO_2$ present white color, and after platinum or gold photochemical deposition a grey or purple powder was obtained respectively.

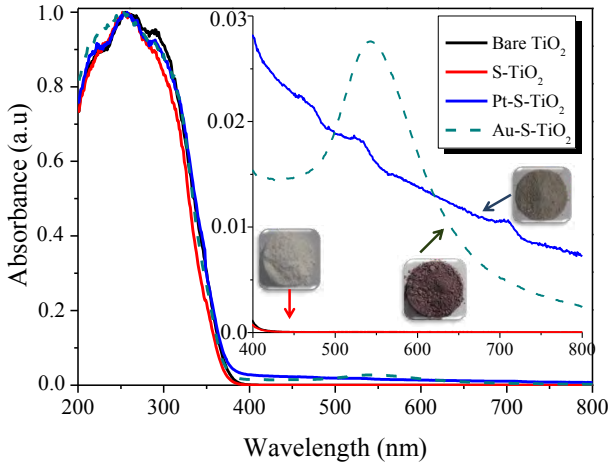


**Figure 2 UV-Vis DRS spectra for bare and metallized $TiO_2$**

Pt-S-$TiO_2$ sample shows optical absorption all over the visible light region (400–700 nm) due to the grey color of this sample (insets in Fig. 2). In this material, three small peaks located at ca. 450, 520 and 700 nm are observed; these peaks can be attributed to the Pt clusters, also can be associated with the visible-light-induced electron transfer from the metal nanoparticles to the $TiO_2$ particle [18]. The Pt nanoparticles deposited on $TiO_2$ can absorb visible light [19]; this visible light photosensitization can be due to the formation of Pt-O-Ti bonds between Pt and $TiO_2$ interface. Here, the surface hydroxyl groups of $TiO_2$ surface play an important role in the chemisorption of Pt complexes and therefore in the formation of the Pt-O-Ti bonds [20]. This assumption is in good correlation with the XPS observations, as it will be seen later.

The absorption of the platinized sample in the visible light region is ascribed to the characteristic optical property of Pt nanoparticles due to the surface plasmon resonance effect in which their conducting electrons undergo a collective oscillation induced by the visible light [18]. Surface plasmon resonance of Pt nanoparticles excited by visible light facilitates the excitation of the surface electron and promotes interfacial electron transfer process, thus improving the $TiO_2$ photoactivity. Similarly, in the visible part of the spectra of the Au-S-$TiO_2$ sample, the surface plasmon resonance band of metallic gold can be observed; this characteristic plasmon is located around 540 nm.

Band gap energy values for all the samples were estimated from the UV–Vis absorption measurements and the obtained values are listed in Table 1. As it can be seen, the band gap of bare $TiO_2$ is close to 3.30 eV, a slight decrease of this value was observed after sulfation and noble metal photochemical deposition.

## X-ray fluorescence

The chemical composition of the samples was analyzed by XRF. For metallized samples, traces of S and $Cl^-$ species coming from the synthesis procedure were detected. Sulfur content in the S-$TiO_2$ sample was 0.66wt.%, in the metallized samples the sulfur and chloride content were under 0.2wt.%. Pt and Au content in the metallized samples was also determined by XRF and it was found to be 0.30wt.% and 0.37wt.% for the Pt-S-$TiO_2$ and Au-S-$TiO_2$ samples, respectively.

As it can be seen, the real metal content in the samples was lower than the nominal content (0.5wt.%) indicating a partial reduction of the metal precursor during the photochemical deposition process carried out under the experimental conditions of this work.

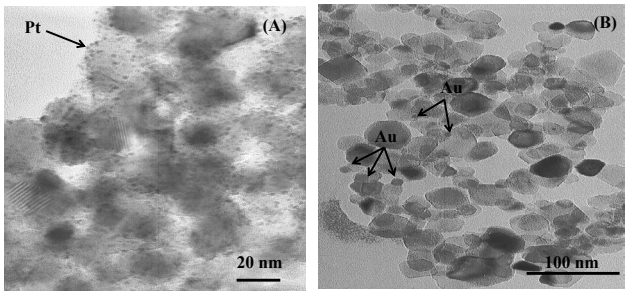


**Figure 3 TEM images of (A) Pt-S-$TiO_2$ and (B) Au-S-$TiO_2$ photocatalysts**

## Transmission Electron Microscopy (TEM)

The morphology of the photocatalysts and metal particle size were analyzed by TEM and representative images of Pt-S-$TiO_2$ and Au-S-$TiO_2$ photocatalysts are presented in Figure 3(a) and 3(b), respectively. As observed in Figure 3(a), the Pt-S-$TiO_2$ sample exhibits uniform distribution of small Pt deposits on $TiO_2$ surface; in this sample the estimated average Pt particle size is 4 nm. On the contrary, in the Au-S-$TiO_2$ sample (Figure 3(b)) the gold particles are heterogeneously located on $TiO_2$ with sizes ranging from 7 nm to diameters larger than 13 nm.

## X-ray photoelectron spectroscopy (XPS)

XPS analyzes were also carried out and the binding energies (BE) of the main XPS peaks (Ti $2p_{3/2}$ and O 1s) for the different samples are enlisted in Table 1. The Ti $2p_{3/2}$ core level spectra were similar for all the analyzed samples with peaks centered at 458.4±0.1 eV, corresponding to $Ti^{4+}$ in the $TiO_2$ network as the main component. In the O 1s region, a peak located at a binding energy of 529.8±0.2 eV was registered in all the samples (Figure 4), this peak is assigned to lattice oxygen (L-$O_2$) in $TiO_2$, with a broad shoulder at higher binding energies ascribed to oxygen in surface hydroxyl groups.

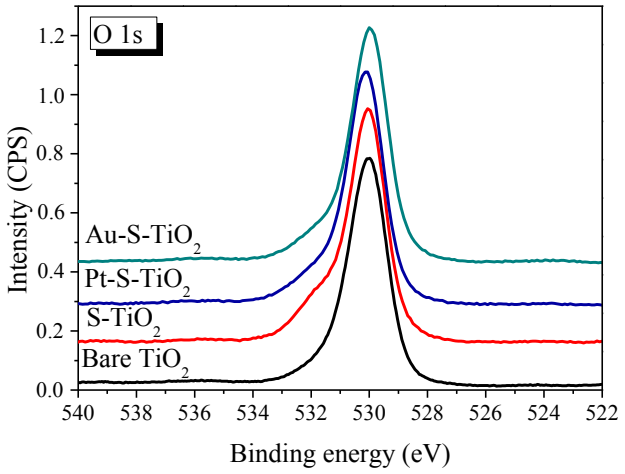


**Figure 4 XPS core level spectra of O 1s region for bare and metallized $TiO_2$**

As it can be seen in Figure 4, this latter shoulder is more pronounced in the S-$TiO_2$ sample, indicating a higher degree of hydroxylation in this material. After Pt or Au photochemical deposition the intensity of this shoulder decreases; this can be due to the high number or metallic particles on $TiO_2$ surface as it was observed in TEM images (Figure 3) which could replace OH groups. Different authors have reported that platinum is chemisorbed on $TiO_2$ through Ti–O–Pt bonds. The formation of these bonds takes place through a condensation reaction between the surface hydroxyl groups on the $TiO_2$ surface and Pt compounds, for that reason the surface hydroxyl groups have an important role for the chemisorption of Pt complexes [20-22].

XPS results in the present study would be in agreement with these authors, as it can be observed that the hydroxylation of $TiO_2$ surface considerably decreases after platinum nanoparticles chemical deposition, suggesting the formation of Pt-O-Ti bonds and affecting also the optical

properties of the platinized $TiO_2$, as it was observed in the UV-Vis DR spectra (Figure 2).

Figure 5 shows the deconvolution of the peaks corresponding to the region of O 1s, performed by the program UNIFIT 2009; in this figure, it is possible to clearly observe the changes in the intensity of the peaks ascribed to hydroxyl groups on photocatalysts surface.

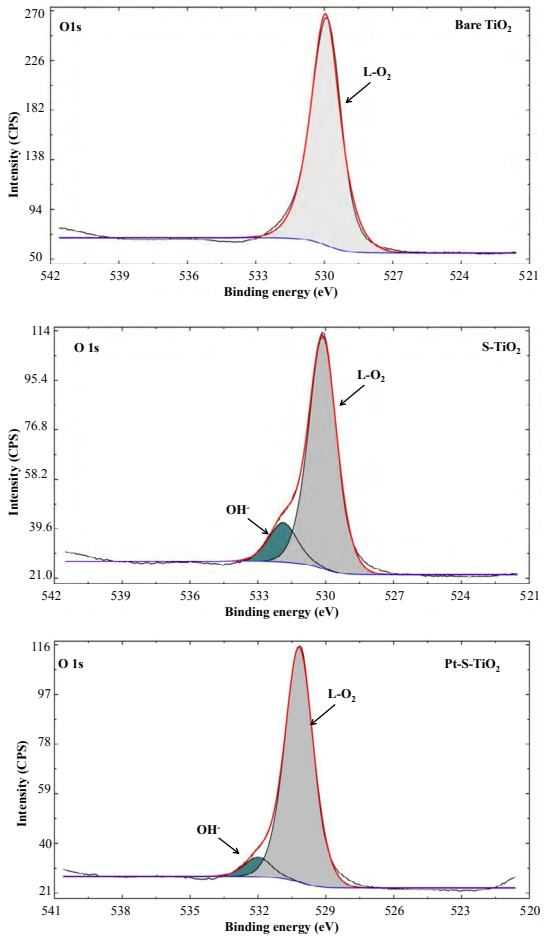


**Figure 5 Deconvolution of the XPS core level spectra of the O 1s for sulfated and platinized $TiO_2$**

From the XPS data, O/Ti ratios were also calculated and the values obtained for all the samples are presented in Table 1. For bare $TiO_2$ the O/Ti value was found to be 1.96, very close to the stoichiometric value (O/Ti = 2). After $TiO_2$ sulfation and calcination treatment, this value considerably decreases being 1.70; indicating the presence of a certain amount oxygen vacancies on the surface of this oxide, in agreement with previous reported results [10] which showed the development of oxygen vacancies on $TiO_2$ surfaces due to the sulfation process. The ratios O/Ti for the metallized samples were higher than the observed in the S-$TiO_2$ sample, suggesting that the oxygen vacancies are partially annihilated during the Pt or Au photochemical deposition over the sulfated oxide.

The determination of the nature and oxidation state of the Pt and Au species can be accomplished by the XPS Pt 4f and Au 4f peaks study. In the case of Pt-S-$TiO_2$ sample, the Pt 4f region is formed by a doublet corresponding to the signals for $4f_{7/2}$ and $4f_{5/2}$, with a binding energy separation of 3.3 eV. The Pt $4f_{7/2}$ binding energy for metallic platinum ($Pt^0$) appears near 70.5 eV, while for oxidized forms ($Pt^{4+}/Pt^{2+}$) appears at higher binding energies with values ca. 74.5 and 72.5 eV, respectively [9].

The Au 4f region is characterized by a doublet of two spin orbit components corresponding to Au $4f_{7/2}$ and Au $4f_{5/2}$ with a separation of about 3.7 eV. The doublet corresponding to metallic gold ($Au^0$) is located at 84.0 eV (Au $4f_{7/2}$) and 87.5 eV (Au $4f_{5/2}$), while oxidized gold doublets appears at higher binding energies ($Au^I$ $4f_{7/2}$ at 84.7 eV and $Au^{III}$ $4f_{7/2}$ at 85.2 eV) [10].

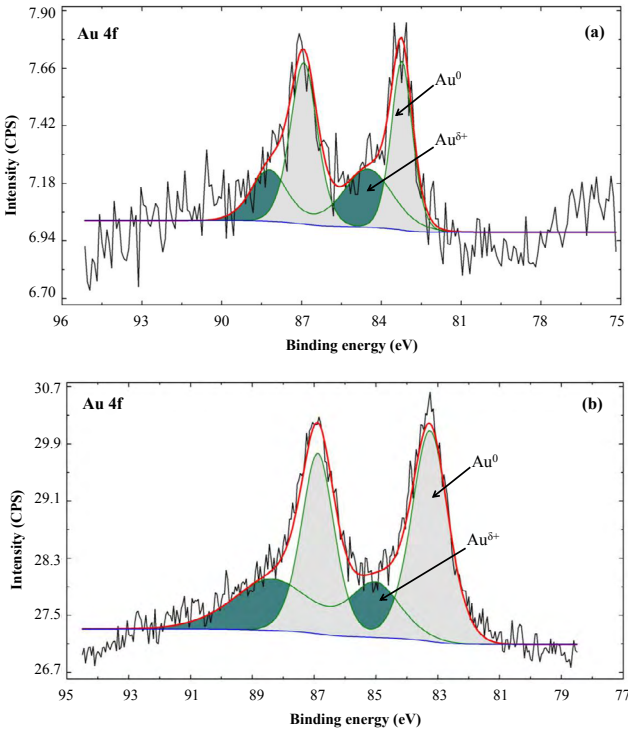


**Figure 6 Deconvolution of the XPS core level spectra of the Au 4f region before (up) and after (down) the first phenol photoreaction recycle under UV-Visible irradiation.**

By means of the deconvolution of the peaks corresponding to the region of Au 4f, using the program UNIFIT 2009, it was possible to make an estimation of the oxidation state of the Au deposits. Figure 6 shows an example of the deconvolution performed for the catalyst Au-S-$TiO_2$. This material was analyzed before (Figure 6(a)) and after (Figure 6(b)) the phenol photoreaction under UV-Visible irradiation. As it can be seen in these figures, the reduction of the noble metal was not completed, appearing a certain fraction of oxidized Au before and after the activity reaction as well. In Figure 6, it is possible to observe qualitatively

that the fraction of oxidized gold does not seem to change significantly during the photoreaction. Some changes in the $Au^0/Au^{\delta+}$ ratio were detected, thus, after photocatalytic reaction, the $Au^0$ percentage slightly increases, being the ratio for these species 70/30 and 73/27 before and after photoreaction, respectively. In can be due to the oxidation of the $Au^0$ species.

For the Pt-S-$TiO_2$ catalyst, it could be assumed, similarly to the Au-S-$TiO_2$ sample that in the analyzed samples there is a certain amount of Pt in an oxidized state, even if the majority of the metal would be present as Pt metallic. This would be in agreement with the results reported previously for 2% Pt-$TiO_2$ catalysts [9].

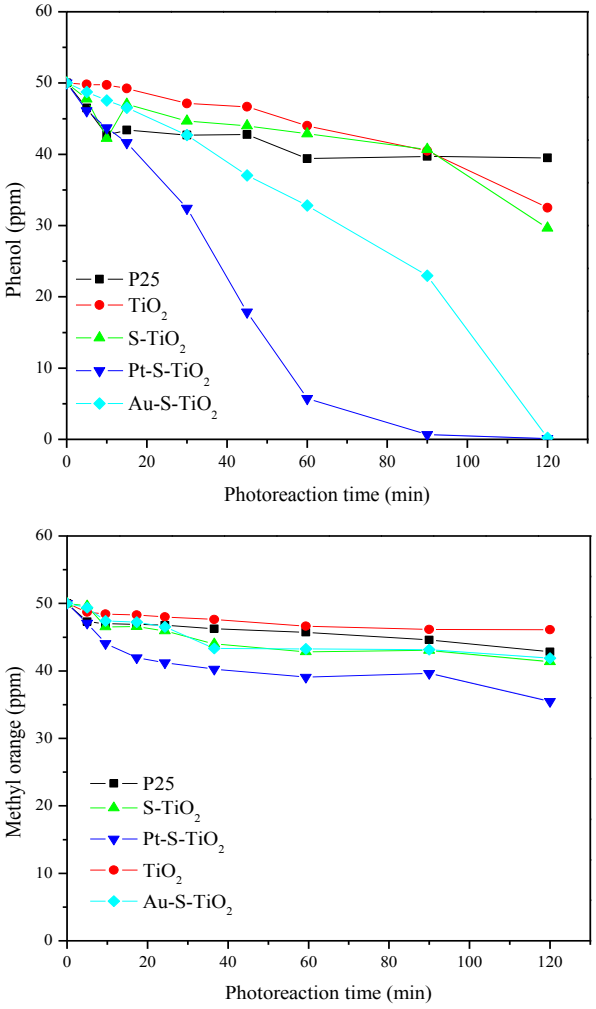


**Figure 7 Pollutant concentration evolution over the analyzed catalysts, under UV-Visible irradiation**

## 3.2. Water pollutants photodegradation reactions

The catalytic activity of the bare and metallized $TiO_2$ was tested in the phenol and methyl orange photodegradation reactions under UV-Visible and only visible light irradiations. Figure 7 shows selected graphs for the phenol and MO concentration evolution under UV-Vis light, as it can be observed, the pollutant concentration decreases with the photoreaction time in all the cases.

Figure 8 shows the initial reaction rates for the phenol degradation over all the analyzed samples under both irradiation conditions. As it can be seen in this figure, the phenol degradation rate under UV-Visible and Visible irradiation increases after $TiO_2$ sulfation. It can be due, among other things, to the highest specific surface area of the S-$TiO_2$ sample compared with the bare $TiO_2$ (Table 1). The increase in the in the visible light activity of $TiO_2$ after sulfation could be explained taking into account that, the calcination of the sulfated $TiO_2$ at 650 °C leads to the formation of oxygen vacancies [9, 10], as it has been indicated by the O/Ti ratio calculated by the XPS data presented before. Oxygen vacancies have been reported to contribute to the absorption of visible light by splitting of the Ti-3d states and generating discrete states about 0.75 eV and 1.18 eV below the conduction band of $TiO_2$ [23-25]. On the other hand, the oxygen vacancies are active electron traps and since the oxygen defect states lie close to the conduction band of $TiO_2$, the electrons captured by oxygen defects can be promoted to the surface where they could be engaged in the degradation of pollutants [5, 24]. All this could explain the visible light activity showed by the S-$TiO_2$ sample for phenol and Methyl orange degradation.

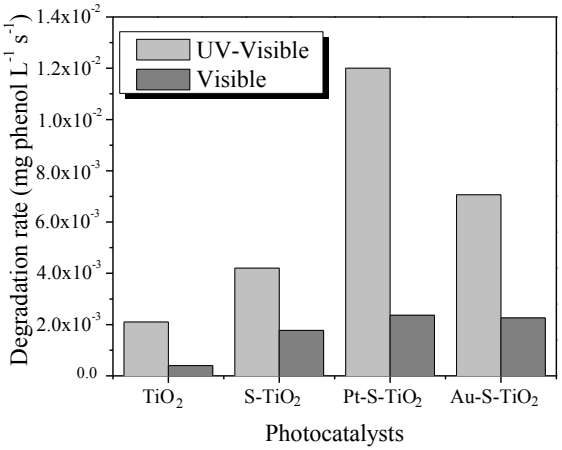


**Figure 8 Initial reaction rates for phenol photodegradation under UV-Vis and visible irradiation, using the photocatalysts analyzed**

All photocatalysts obtained by $TiO_2$ modification with noble metal nanoparticles deposition revealed a higher degradation rate of phenol (Figure 8) and Methyl Orange (Figure 9) compared to bare and sulfated $TiO_2$, under UV-Vis illumination and under visible illumination as well. However, as it can be seen in these figures, the initial degradation rate of the substrates obtained by using Au-S-$TiO_2$ as photocatalyst, is lower than the obtained with the Pt-S-$TiO_2$ sample, and even lower than the obtained with the S-$TiO_2$ sample, in the case of the methyl orange (Figure 9).

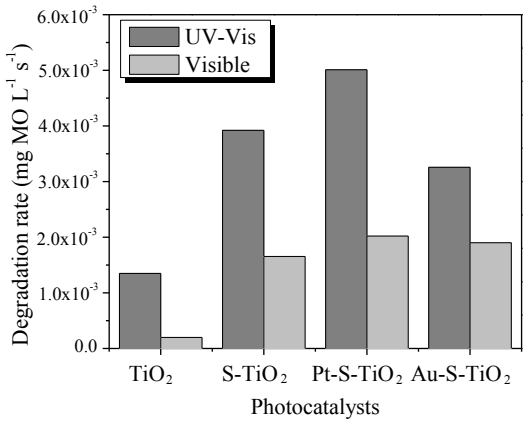


**Figure 9 Initial reaction rates for methyl orange photo-degradation under UV-Vis and visible irradiation, using the photocatalysts analyzed**

In general, the dye photodegradation rate obtained over all the analyzed catalysts was lower than the observed in the phenol degradation; it could be due to a screening effect of the dye over the catalysts photoactivity. It is also important to take into account that the pollutants degradation efficiency depends on different factors such as the kind or structure of the substrate to be degraded. Thus, some molecules can be adsorbed on the photocatalyst surface by different mechanisms or ways, as it has been previously reported by Murcia *et al.* [9].

The commercial $TiO_2$ Aeroxide Evonik P25 was also tested under UV- visible light and it shows a lower photocatalytic degradation rate than the metallized $TiO_2$, rates of $2x10^{-3}$ and $6.8x10^{-4}$ $mg.L^{-1}.s^{-1}$ were obtained for phenol and methyl orange degradation, respectively.

Best photocatalytic performance for both tested reactions is given by the platinized sample (Pt-S-$TiO_2$). The high dispersion and small particle size Pt deposits presented in this sample are surely responsible for this high activity. As it has been widely reported, Pt deposits on $TiO_2$ can act as efficient traps for the photogenerated electrons, thus decreasing the electro-hole pair recombination rate during the photocatalytic process. This mechanism of efficiency improvement is enhanced by a high dispersion and small size of the Pt particles [9, 26].

In the case of the sample with Au, the improvement of activity is less notable than for the Pt counterpart. For Au-S-$TiO_2$, metal particles are much more heterogeneous distributed and present larger sizes than Pt deposits in Pt-S-$TiO_2$, what certainly is less effective in the mechanism of electron trapping.

Under visible illumination, metallized samples present also a higher rate for phenol and methyl orange degradation than S-$TiO_2$. In this case, visible light absorption by the noble metal plasmonics could also be taking place. Plasmonic metal nanoparticles on $TiO_2$ could act similarly to a dye sensitizer, absorbing resonant photons and transferring the electron formed in the process of the surface plasmon resonance excitation to the semiconductor; in this mechanism the electron could react with $O_2$ or oxidants and the hole could react with $OH^-$ to produce active radicals which subsequently degrade the water pollutants [1, 27, 28].

In general, for both substrates the photoactivity of the materials analyzed increases in the following order: bare $TiO_2$<<<S-$TiO_2$<Au-S-$TiO_2$<Pt-S-$TiO_2$. Measurements of Total Organic Carbon (TOC) showed that practically total mineralization of phenol (0.02–0.04 mg/L TOC) was reached after 120min of reaction for the Pt-S-$TiO_2$ sample.

The best photocatalyst was evaluated under direct solar light and under the environmental condition of the city of Tunja (Boyacá), Colombia (5°32′7″North latitude 73°22′04″E), the results obtained are shown in Figure 10. Over each bar, the solar light intensity is indicated. As it can be observed, the platinized catalysts is also active under solar light; as expected, the pollutants photodegradation rate obtained under solar light is lower than the observed under artificial light, this is mainly due to the lowest sunlight intensity; however, the results obtained in the present research can be a starting point for the design of an optimized photocatalytic reactor, working efficiently under sunlight, taking advantage of the effectiveness of platinized catalysts in the water pollutant photodegradation.

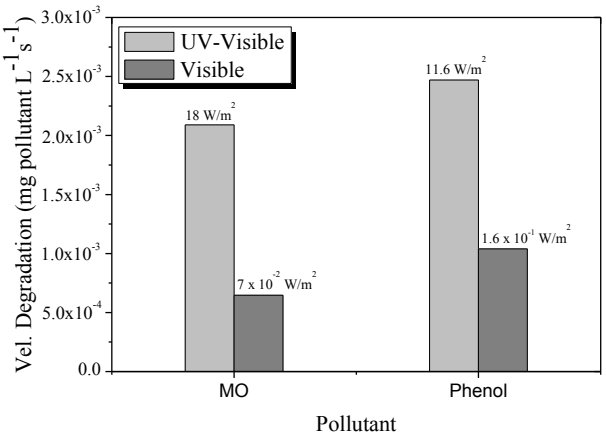


**Figure 10 Initial reaction rates for phenol and Methyl orange photodegradation over Pt-S-$TiO_2$ photocatalyst using direct solar light**

The irradiation power according to the surface area was calculated for the photocatalytic tests carried out under sunlight and artificial light, then the Phenol or Methyl orange degradation rate was normalized per irradiation power, these results are presented in Figure 11. As it can be seen in this figure, the global efficiency of the photocatalytic treatment for these substrates increases with the light intensity, by using the Pt-S-$TiO_2$ photocatalyst.

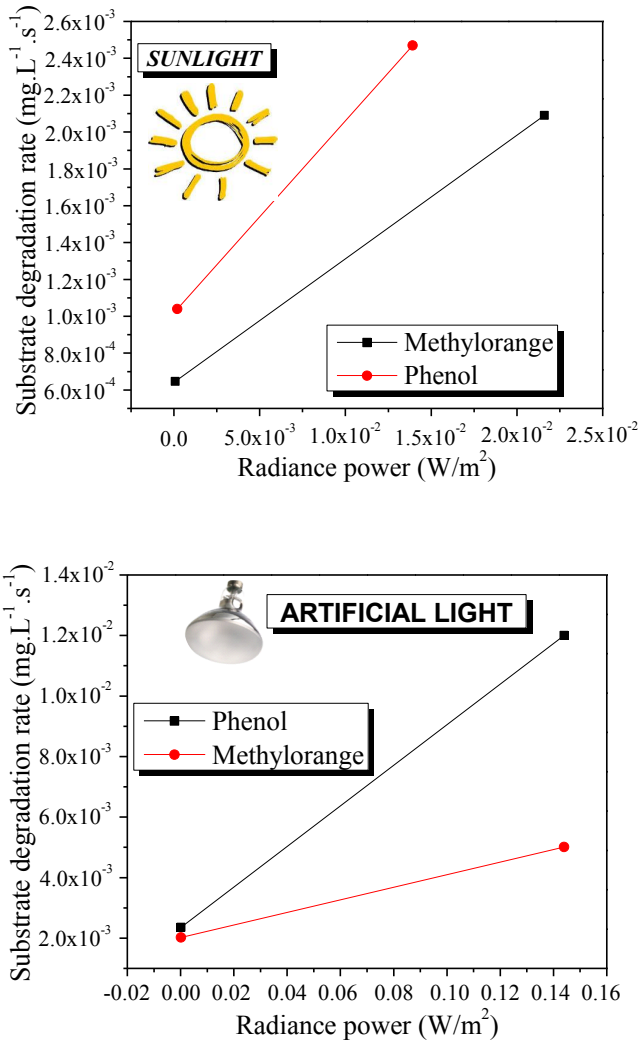


**Figure 11** Initial reaction rates for substrates photodegradation over Pt-S-$TiO_2$ photocatalyst using artificial and sunlight

## 3.3. Recycling of metallized photocatalysts in phenol photodegradation reaction

In order to evaluate the stability of the metallized photocatalysts Pt-S-$TiO_2$ and Au-S-$TiO_2$ under UV-Visible light irradiation, both samples were reused in a subsequent cycle of phenol photodegradation. The recycling experiments were performed using renewed phenol solution where the catalysts had been recovered after photoreaction by filtration, washing and drying. In all the tests, 1g/L of photocatalyst was employed. Figure 12 shows a comparison of the phenol degradation rates in the different runs. As observed in this figure, there was no decrease of the degradation rate of the Pt-S-$TiO_2$ photocatalyst after the second reaction, indicating the good stability this material.

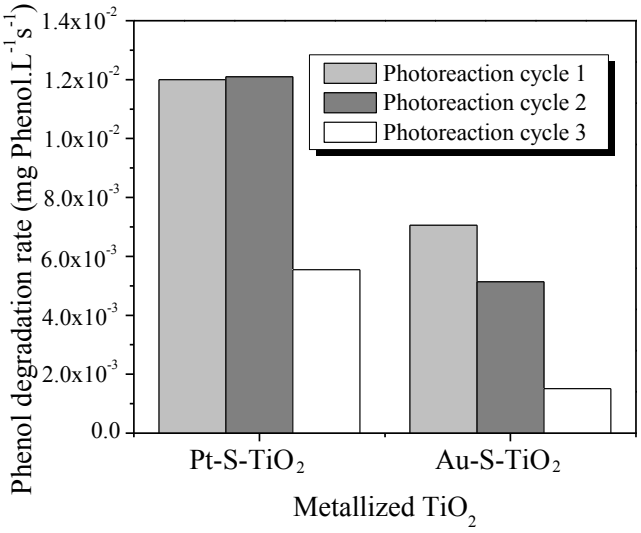


**Figure 12** Initial reaction rates for phenol photodegradation under UV-Visible irradiation, after recycling of the metallized photocatalysts

In the case of the Au-S-$TiO_2$ catalyst, the photoreaction rate considerably decreases after the first reaction cycle. This decreasing of the photocatalytic activity observed in the Au-S-$TiO_2$ after phenol degradation reaction could be mainly due to the obstruction of the active sites on the surface of the catalysts by the phenol degradation intermediates which are difficult to remove after the photoreactions [29], it can be also due to the catalyst degradation after reaction. It is important to consider that Pt or Au nanoparticles could be oxidized by the holes and/or surface hydroxyl radicals generated during photocatalysis. In order to determine a possible oxidation of the metallic species, XPS analyzes of the metallized samples after the phenol photodegradation were carried out and it was observed that the oxidation state of the Pt or Au species was not modified after photoreaction, as it was seen in Figure 6.

On the other hand, no lixiviation of the platinum during the photodegradation reaction was detected, since the content of the metal in the Pt-S-$TiO_2$ catalyst was the same before and after the photocatalytic cycle as it was found by the XRF analysis. However, in the case of the Au-S-$TiO_2$ photocatalyst, it was observed a decrease in the gold content after the first cycle of reaction, being gold content in the sample 0.37% before and 0.30% after the first photoreaction. This could also contribute to the decrease of photoactivity observed for this sample after the first reaction test.

# 4. Conclusions

A notable visible light activity for phenol and Methyl Orange degradation was observed for sulphated $TiO_2$ and for metallized sulphated $TiO_2$.

Visible light activity of S-$TiO_2$ could be ascribed to the presence of a high number of oxygen vacancies present in

the sample. Pt or Au deposited on sulphated $TiO_2$ also led to visible active samples, increasing the visible degradation rates for both tested reactions.

The Pt-S-$TiO_2$ photocatalysts have demonstrated to be active under artificial light source and also under sunlight and the environmental conditions of a Colombian region, where the light intensity used to be lower, but with many hours of light during the day.

Recycling of the catalysts showed that Pt-S-$TiO_2$ was more stable sample than Au-S-$TiO_2$ for phenol photodegradation.

## 5. Acknowledgements

This work was financed by Fondo Nacional de Financiamiento para la Ciencia, la Tecnología y la Innovación "Fransisco José de Caldas – Colciencias", Project 279-2016 and Universidad Pedagógica y Tecnológica de Colombia. This work was partially supported by research fund from Project Ref. CTQ2015-64664-C2-2-P (MINECO/FEDER, UE).

## 6. References

1. M. Pelaez *et al.*, "A review on the visible light active titanium dioxide photocatalysts for environmental applications," *Appl. Catal. B.*, vol. 125, pp. 331– 349, 2012.
2. S. Malato, P. Fernández, M. I. Maldonado, J. Blanco, and W. Gernjak., "Decontamination and disinfection of water by solar photocatalysis: Recent overview and trends," *Catal. Today.*, vol. 147, no. 1, pp. 1–59, 2009.
3. S. G. Kumar and L. G. Devi, "Review on Modified $TiO_2$ Photocatalysis under UV/Visible Light: Selected Results and Related Mechanisms on Interfacial Charge Carrier Transfer Dynamics," *J. Phys. Chem. A.*, vol. 115, no. 46, pp. 13211–13241, 2011.
4. T. Fotiou, T. M. Triantis, T. Kaloudis, and A. Hiskia, "Evaluation of the photocatalytic activity of $TiO_2$ based catalysts for the degradation and mineralization of cyanobacterial toxins and water off-odor compounds under UV-A, solar and visible light," *Chem. Eng. J.*, vol. 261, pp. 17–26, 2015.
5. S. Rehman, R. Ullah, A. M. Butt, and N. D. Gohar, "Strategies of making $TiO_2$ and ZnO visible light active," *J. Hazard. Mater.*, vol. 170, no. 2-3, pp. 560–569, 2009.
6. A. A. Ashkarran, H. Hamidinezhad, H. Haddadi, and M. Mahmoudid, "Double-doped $TiO_2$ nanoparticles as an efficient visible-light-activephotocatalyst and antibacterial agent under solar simulated light," *Appl. Surf. Sci.*, vol. 301, pp. 338–345, 2014.
7. S. H. Hsieh, W. J. Chen, and C. T. Wu, "Pt-$TiO_2$/graphene photocatalysts for degradation of AO7 dye under visible light," *Appl. Surf. Sci.*, vol. 340, pp. 9–17, 2015.
8. S. Neubert *et al.*, "Surface-Modified $TiO_2$ Photocatalysts Prepared by a Photosynthetic Route: Mechanism, Enhancement, and Limits," *ChemPlusChem.*, vol. 79, no. 1, pp. 163–170, 2014.
9. J. J. Murcia, M. C. Hidalgo, J. A. Navío, J. Araña, and J. M. Doña, "Correlation study between photo-degradation and surface adsorption properties of phenol and methyl orange on $TiO_2$ Vs platinum-supported $TiO_2$," *Appl. Catal. B.*, vol. 150–151, pp. 107–115, 2014.
10. M. Maicu, M.C. Hidalgo, G. Colón and J.A. Navío, "Comparative study of the photodeposition of Pt, Au and Pd on pre-sulphated $TiO_2$ for the photocatalytic decomposition of phenol," *J. Photochem. Photobiol. A.,* vol. 217, pp. 275-283, 2011.
11. N. M. Thuy, D. Q. Van, and L. T. Hong, "The Visible Light Activity of the $TiO_2$ and $TiO_2$:$V^{4+}$ Photocatalyst," *Nanomater. Nanotechnol.,* vol. 2, pp. 1–8, 2012.
12. S. W. Verbruggen *et al.*, "Plasmonic gold–silver alloy on $TiO_2$ photocatalysts with tunable visible light activity," *Appl. Catal. B.*, vol. 156–157, pp. 116–121, 2014.
13. A. Golabiewska *et al.*, "Visible light photoactivity of $TiO_2$ loaded with monometallic (Au or Pt) and bimetallic (Au/Pt) nanoparticles," *Appl. Surf. Sci.*, vol. 317, pp. 1131–1142, 2014.
14. N. Lakshminarasimhan, A. D. Bokare, and W. Choi, "Effect of Agglomerated State in Mesoporous $TiO_2$ on the Morphology of Photodeposited Pt and Photocatalytic Activity," *J. Phys. Chem. C.*, vol. 116, no. 33, pp. 17531–17539, 2012.
15. S. Semlali *et al.*, "Mesoporous Pt-$TiO_2$ thin films: Photocatalytic efficiency under UV and visible light," *Appl. Catal. B.*, vol. 150–151, pp. 656– 662, 2014.
16. K. Okazaki, Y. Morikawa, S. Tanaka, K. Tanaka, and M. Kohyama, "Effects of stoichiometry on electronic states of Au and Pt supported on $TiO_2$ (110)," *J. Mater. Sci.*, vol. 40, no. 12, pp. 3075–3080, 2005.
17. L. C. Chen, F. R. Tsai, and C. M. Huang, "Photocatalytic decolorization of methyl orange in aqueous medium of $TiO_2$ and Ag–$TiO_2$ immobilized on γ-$Al_2O_3$," *J. Photochem. Photobiol. A.,* vol. 170, no. 1, pp. 7–14, 2005.
18. Z. Zheng *et al.*, "Facile in situ synthesis of visible-light plasmonic photocatalysts M@$TiO_2$ (M = Au, Pt, Ag) and evaluation of their photocatalytic oxidation of benzene to phenol," *J. Mater. Chem.*, vol. 21, no. 25, pp. 9079–9087, 2011.
19. B. Wang *et al.*, "Fabrication and enhanced visible-light photocatalytic activity of Pt-deposited $TiO_2$ hollow nanospheres," *Chem. Eng. J.* vol. 223, pp. 592–603, 2013.
20. Y. Ishibai, J. Sato, T. Nishikawa, and S. Miyagishi, "Synthesis of visible-light active $TiO_2$ photocatalyst with Pt-modification: Role of $TiO_2$ substrate for high photocatalytic activity," *Appl. Catal. B.*, vol. 79, no. 2, pp. 117–121, 2008.
21. W. Macyk and H. Kisch, "Photosensitization of Crystalline and Amorphous Titanium Dioxide by Platinum(IV) Chloride Surface Complexes," *Chem. Eur. J.*, vol. 7, no. 9, pp. 1862–1867, 2001.
22. R. Palmans and A. J. Frank, "A molecular water-reduction catalyst: surface derivatization of titania colloids and suspensions with a platinum complex," *J. Phys. Chem.*, vol. 95, no. 23, pp. 9438–9443, 1991.

23. J. Ma, H. Wu, Y. Liu, and H. He, "Photocatalytic Removal of NOx over Visible Light Responsive Oxygen-Deficient $TiO_{2,}$" *J. Phys. Chem. C.*, vol. 118, no. 14, pp. 7434-7441, 2014.
24. I. Nakamura *et al.*, "Role of oxygen vacancy in the plasma-treated $TiO_2$ photocatalyst with visible light activity for NO removal," *J. Mol. Catal. A: Chem.*, vol. 161, no. 1-2, pp. 205–212, 2000.
25. T. Ihara, M. Miyoshi, Y. Iriyama, O. Matsumoto, and S. Sugihara, "Visible-light-active titanium oxide photocatalyst realized by an oxygen-deficient structure and by nitrogen doping," *Appl. Catal. B*. vol. 42, no. 4, pp. 403–409, 2003.
26. A. A. Ismail and D. W. Bahnemann, "Mesostructured Pt/$TiO_2$ Nanocomposites as Highly Active Photocatalysts for the Photooxidation of Dichloroacetic Acid," *J. Phys. Chem. C.*, vol. 115, no. 13, pp. 5784–5791, 2011.
27. S. Linic, P. Christopher, and D. B. Ingram, "Plasmonic-metal nanostructures for efficient conversion of solar to chemical energy," *Nat. Mater.*, vol. 10, no. 12, pp. 911–921, 2011.
28. N. Pugazhenthiran, S. Murugesan, P. Sathishkumar, and S. Anandan, "Photocatalytic degradation of ceftiofur sodium in the presence of gold nanoparticles loaded $TiO_2$ under UV–visible light," *Chem. Eng. J.*, vol. 241, pp. 401–409, 2014.
29. E. Grabowska, J. Reszczynska, and A. Zaleska, "Mechanism of phenol photodegradation in the presence of pure and modified-$TiO_2$: A review," *Water Res.*, vol. 46, no. 17, pp. 5453 – 5471, 2012.